Research Article

Journal of Environmental Nanotechnology

Synthesis and Characterization of Pure and Copper-doped HAp Nanoparticles by Microwave Irradiation Method

K. Mohanapriya*, N. Vidhya, V. Kalaiselvi, K. Surya, V. Ramya
Department of Physics, Navarasam Arts and Science College for Women, Erode, TN, India
Received: 20.03.2020 Accepted: 22.04.2020 Published: 30-09-2020
*mohanapriya98k@gmail.com

ABSTRACT

Hydroxyapatite (HAp) is a nano biomaterial incorporated as bone and teeth implants in the human body. In the present work, HAp was prepared using calcium hydroxide as a calcium source and orthophosphoric acid as a phosphorous source by chemical co-precipitation method associated with microwave irradiation method. Pure and copper-doped HAp nanoparticles were synthesized by chemical co-precipitation method associated with microwave irradiation method. The prepared copper-doped HAp was characterized by XRD, FTIR, SEM, EDAX, UV and PL techniques. The X-ray Diffraction (XRD) pattern had revealed the crystalline size of the nanoparticles. The Fourier Transform Infrared Spectroscopy (FTIR) pattern had given the functional groups. Morphology and purity of the sample were analyzed by Scanning Electron Microscopy (SEM) and Energy Dispersion X-ray Diffraction (EDAX). The optical properties were ascertained by using Ultra-Violet spectroscopy (UV) and Photo Luminance spectroscopy (PL). The results obtained matched well with the standard values.

Keywords: Copper-doped hydroxyapatite; Co-precipitation method; Crystalline size; Morphology; Optical properties; Pure hydroxyapatite**.**

1. INTRODUCTION

Nanotechnology is the study of extremely small structures, having a size of 0.1 to 100 nm. Nanomedicine is a relatively new field of science and technology (Uota *et al.* 2005). Nanotechnology has applications in various fields (Shi *et al.* 2009) such as health and medicine, electronics, energy and environment. Nanoparticles are used in drug delivery, protein and peptide delivery (Ratanatawanate *et al.* 2011). Various nanosystems are applied in cancer therapy such as carbon nanotube, dendrimers, nanocrystal, nanowire and nanoshells (Venkatasubbu *et al.* 2013; Simon *et al.* 2019).

Calcium hydroxide has been included within several materials and antimicrobial formulations that are used in a number of treatment modalities in endodontics (Nikalje *et al.* 2015). Calcium hydroxide formulations are also used during the treatment of root perforations, root fractures and root resorption and have a role in dental traumatology (Haresh M. Pandya *et al.* 2017). Phosphoric acid, also known as orthophosphoric acid, is a triprotic acid that exists as a dense liquid. It is an irritant or corrosive to the skin, eyes and other mucous membranes of both humans and laboratory animals. Copper sulphate is an inorganic compound that combines sulphur with copper (Kalaiselvi *et al.* 2017) . It can kill bacteria, algae, roots, plants, snails and fungi. The toxicity of copper sulphate depends on the copper content. Copper is an essential mineral (Gonzalez-McQuire *et al.* 2004).

In the present study, Copper-doped HAp nanoparticles were used for the chemical synthesis of Cu-HAp nanoparticles under different physical conditions. The synthesized Cu-HAp nanoparticles were characterized by Scanning Electron Microscopy (SEM), Electron Dispersive X-Ray analysis (EDAX), Fourier Transform Infrared Spectroscopy (FTIR), X-Ray Diffraction (XRD), UV-Visible Spectroscopy (UV-Vis.), and Photo Luminance Spectroscopy (PL).

2. MATERIALS & METHODS

2.1 Preparation of Pure HAp Nanoparticles

The pure HAp nanoparticles were synthesized by the co-precipitation method. 3.705 g of calcium hydroxide was dissolved in 50 ml of distilled water. Then, 2.94 g of orthophosphoric acid was dissolved in 50 ml of distilled water. Both solutions were stirred for 30 min. in separate beakers. Then orthophosphoric acid was added to the calcium hydroxide solution, the mixture was allowed to get stirred for 30 min. The NaOH solution was added drop-by-drop into the solution to maintain pH up to 12 (Mohammadi *et al.* 2011). Then the solution was

stirred 30 min. After 30 min., the solution was subjected to ageing for one day at room temperature. The settled precipitate was washed by distilled water and dried in a microwave oven at 75 W for 20 min. The dried sample was grained in mortar. The mixture was kept in a muffle furnace at 4 hours, to get a white colour pure hydroxyapatite nano powder (Kalaiselvi *et al.* 2017; 2018).

2.2 Synthesis of Cu-HAp Nanoparticles

The Cu-doped HAp nanoparticles were synthesized by the co-precipitation method. 3.705 g of calcium hydroxide was dissolved in 50 ml of distilled water. Then, 2.94 g of orthophosphoric acid was dissolved in 50 ml of distilled water. 0.6242 g of copper was dissolved in 50 ml of distilled water. These solutions were stirred for 30 min. in separate beakers. After 30 min., orthophosphoric acid was added with calcium hydroxide solution, it was allowed to stir for 30 minutes. Further, the copper solution was added to the above mixture and allowed to stir for 30 minutes. Then the NaOH solution was added to maintain the pH up to 12. Then the solutions were agitated for 30 minutes and allowed for ageing for one day at room temperature. The water was removed and dried in the microwave oven at 75 W for 20 minutes. The dried sample was grained in mortar. The mixture was kept in a muffle furnace for 4 hours, to get Copper-doped hydroxyapatite nanopowder.

2.3 Characterization Techniques

2.3.1 X-Ray Diffraction (XRD)

X-ray diffraction (XRD) relies on the dual wave/particle nature of X-rays to obtain information about the structure of crystalline materials. The lattice parameter of the sample was calculated using the following equation:

$$1/d^2 = (4(h^2+hk+k^2)/3a) + (1^2/c^2)$$

where, d is the spacing between the planes and a and c are the lattice parameters. The unit cell volume (V) of the sample was described using the equation:

$$V = (\sqrt{3}/2) + a^2 + c^2$$

The average crystalline size of the sample was determined by using Scherer's formula.

$$D = K\lambda/\beta\cos\theta$$

where, D denotes the average crystalline size of the sample, K represents the broadening constant, λ denotes the wavelength of CuKα radiation source (1.54 A^0), β represents full width at half-maximum and θ denotes angle of diffraction.

2.3.2 SEM and EDAX

The surface morphologies of synthesized Cu-HAp samples were analysed using SEM. EDAX was used to identify the elemental composition of the sample.

3. RESULTS

3.1 SEM analysis

The morphological structure of the prepared nanocomposites was revealed in SEM. These analyses are useful in the crystalline structure, chemical composition and crystal orientations. Fig. 3 (a) shows pure HAp nanoparticles and Fig. 3 (b) shows Cu-doped HAp nanoparticles. Pure HAp nanoparticles showed cluster-like structure, whereas Cu-doped HAp nanoparticles non-uniform cluster-like structure. The formation of pure HAp was found to be 27.69 - 46.28 nm. The formation of Cu-doped HAp was found to be 55.54 – 71.72 nm.

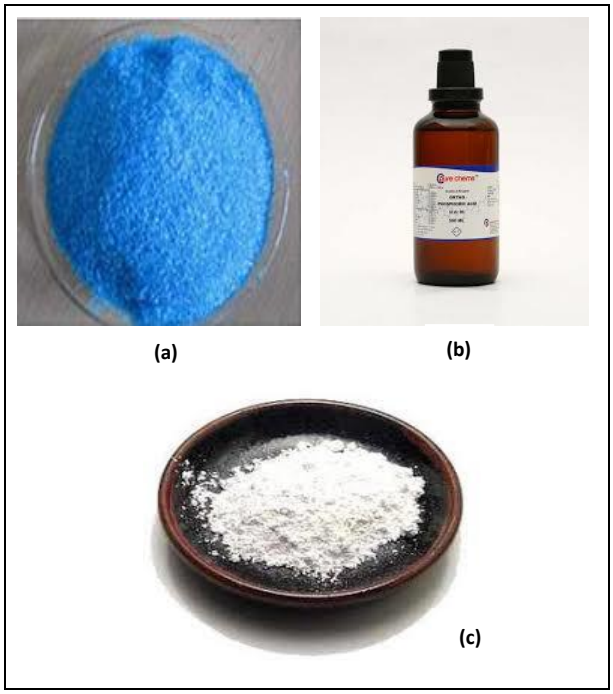

Fig. 1: (a) Copper sulphate (b) Orthophosphoric acid (c) Calcium hydroxide.

3.2 XRD Analysis

The XRD pattern of prepared pure HAp nanoparticles was shown in Fig. 2. The crystalline size of the nanoparticles was determined from the peak value. The average crystalline size calculated using Debye-Scherrer formula is approximately in the range between 5-24 nm (Table 1).

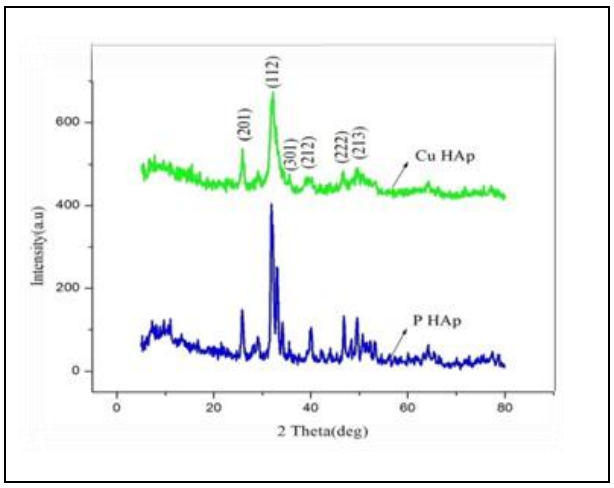

Fig. 2: XRD analyses of pure HAp and Cu-HAp nanoparticles.

3.3 EDAX Analysis

The EDAX analysis has shown peaks corresponding to the elements making up the true composition of the sample being analyzed, elemental mapping of a sample and image analysis (Table 2 & Fig. 4).

3.4 FTIR:

The characteristic bands present in the sample were predicted by FTIR spectra. The presence of phosphate and hydroxyl groups were identified, which corresponds to HAp structure. The FTIR spectrum of HAp shows the vibration modes of phosphate at 870.70, 570.82 and 1044.26 cm^{-1}. Hydroxyl groups of HAp was revealed at 3454.85 cm^{-1} and 3744.12 cm^{-1}. The vibration modes at 569.86, 872.631 and 1043.31 cm^{-1} revealed the presence of phosphate and Hydroxyl groups at 3456.78 and 3636.12 cm^{-1} for Cu-HAp. Peaks at 1421.28 and 1420.32 cm^{-1} represented the CH_3 stretching of carboxylic acid. The present groups were shown in Table 3 and Fig. 5.

Table 1. XRD analyses of pure HAp and Cu-HAp nanoparticles.

Sample	2θ (deg)	FWHM (deg)	D (A^0)	Intensity (counts)	Crystalline size (nm)	Average crystalline size (nm)	hkl	Lattice constants		Unit Volume
								a = b	c	
	25.84	0.5629	3.44	68	14.57		201			502.83
	31.97	0.7205	2.79	226	11.47		112			546.46
	35.97	0.3467	2.52	11	21.11		301			524.98
Pure HAp	39.10	0.4000	2.30	10	24.06	17.51	212	9.38	6.89	532.84
	42.25	0.4834	2.13	13	17.61		311			525.77
	46.81	0.5035	1.93	58	17.19		222			524.98
	49.50	0.5284	1.83	56	16.55		213			526.50
	25.87	0.92	3.44	35	8.80		201			504.27
	32.21	1.56	2.77	134	5.27		112			523.86
	35.00	1.20	2.53	15	6.95		301			512.87
Cu-HAp	39.55	1.90	2.27	18	4.39	7.91	212	9.35	6.86	511.63
	41.95	0.50	2.15	4	16.99		311			530.59
	46.65	1.10	1.94	22	7.86		222			530.23
	49.40	1.70	1.84	29	5.14		213			531.71

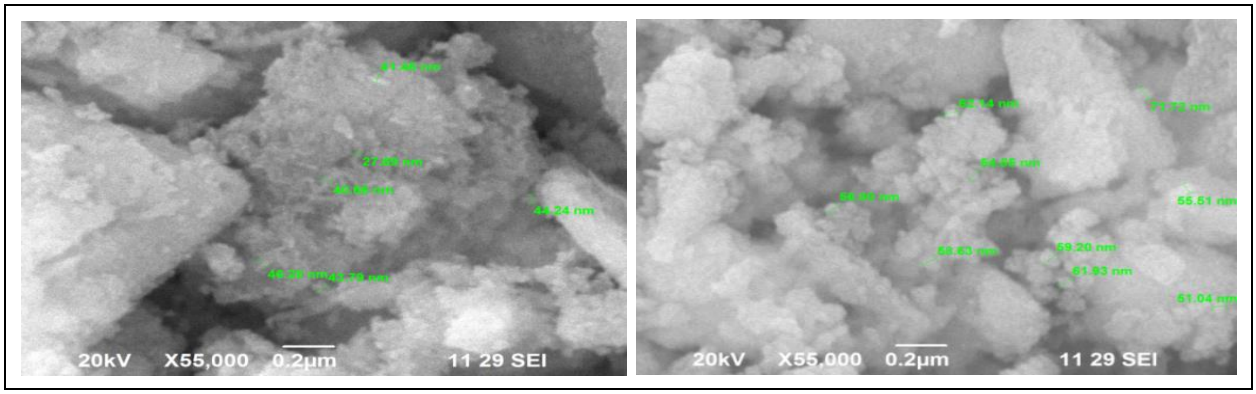

Fig. 3: SEM image of: (a) Pure HAp and (b) Cu-doped HAp nanoparticles.

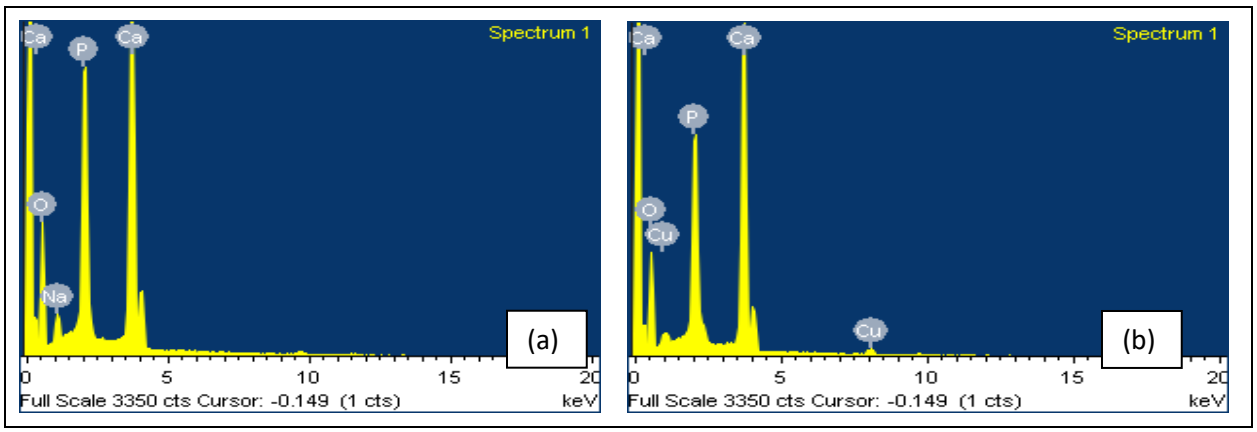

Fig. 4: EDAX image for pure and Cu-HAp nanoparticles.

Table 2. EDAX analyses of pure and Cu-HAp nanoparticles.

Sample	Element	Weight %	Atomic %
Pure HAp	O K	51.23	70.08
	Na K	2.93	2.79
	P K	13.05	9.22
	Ca K	32.79	17.91
Cu-HAp	O K	52.90	72.61
	P K	13.28	9.41
	Ca K	31.11	17.04
	Cu K	2.71	0.94

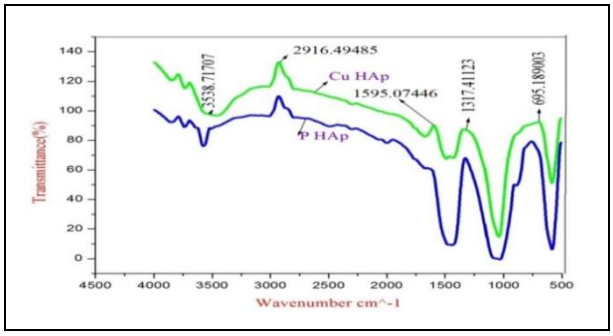

Fig. 5: FTIR images of pure-HAp and Cu-HAp nanoparticles.

Table 3. FTIR analyses of pure HAp and Cu-HAp nanoparticles.

S. No.	Sample	Wave Number, cm^{-1}				
		O-H stretching vibration	C-H stretching vibration	C=C stretching vibration	CH_3 stretching vibration	P-O Stretching vibration
1	Pure HAp	3555.67	2918.55	1593.81	1319.58	694.84
2	Cu-HAp	3538.71	2916.49	1595.07	1317.41	695.18

3.5 UV Analysis

UV–Vis. spectroscopy examined the sample's optical properties and bandgap energy. The wavelength spectrum of 310 nm was present in the absorption spectra of pure HAp and Cu-HAp nanoparticles. HAp and Cu-HAp had a bandgap energy of 4.00 eV. Due to quantum size effects and electronic structure changes, both samples have the same wavelength and bandgap energy. Table 4 shows the energy band and wavelength of the particles. The spectra of pure HAp and Cu-HAp were shown in Fig. 6 and bandgap energies were given in Table 4.

Table 4. Band gap energy of pure HAp and Cu-HAp nanoparticles.

S. No.	Sample	Wavelength (nm)	Bandgap energy (eV)
1	Pure HAp	310	4.00
2	Cu-HAp	310	4.00

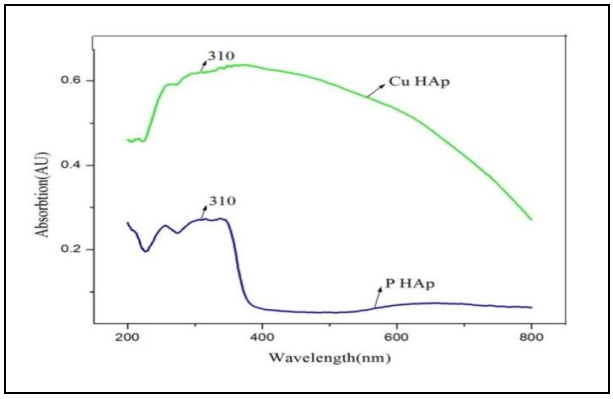

Fig. 6: UV-Vis images of pure and Cu-doped HAp nanoparticles.

3.6 Photoluminescence spectroscopy

The intensity of emission radiations was observed by Photoluminescence spectroscopy. The

emission radiation of HAp and Cu-HAp were shown in Fig. 7. The excitation wavelength has occurred at the range of 228.34 nm for both HAp and Cu-HAp. The emission band of Cu-HAp was located at 310.9 nm. In HAp, there was no shift present at the range. The standard bandgap energy of HAp was around the range of 3.45 to 5.40 eV, while the calculated bandgap energy of both the samples is 3.189 eV.

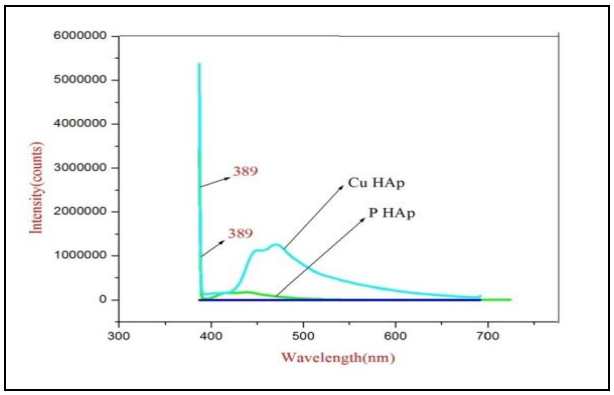

Fig. 7: PL analyses of pure HAp and Cu-HAp nanoparticles.

4. CONCLUSION

Microwave irradiation was used to irradiate hydroxyapatite nanoparticles, which were green synthesized. The XRD pattern verified the sample's crystalline dimension, lattice parameters and nanoparticle unit cell length. When comparing Cu-HAp to HAp, the crystalline scale decreased. The existence of functional groups can be seen in the FTIR spectrum, verifying the presence of phosphate and hydroxyl groups in the sample. UV-Vis. was used to determine the bandgap energy and wavelength; HAp and Cu-HAp had a bandgap energy of 4.00 eV. The morphological structure of spherical shape was predicted by SEM research. The occurrence of calcium and phosphate groups in the ratio of 1.65 was confirmed by EDAX research. The sample's bandgap energy and optical absorption were shown by UV and PL analyses. The measured bandgap energy was 4.00 eV.

FUNDING

This research received no specific grant from any funding agency in the public, commercial, or not-for-profit sectors.

CONFLICTS OF INTEREST

The authors declare that there is no conflict of interest.

COPYRIGHT

REFERENCES

Gonzalez-McQuire, R., Chane-Ching, J.-Y., Vignaud, E., Lebugle, A. and Mann, S., Synthesis and characterization of amino acid-functionalized hydroxyapatite nanorods, *J. Mater. Chem.*, 14(14), 2277 (2004). https://dx.doi.org/10.1039/B400317A

Haresh M. Pandya, Anitha, P., Mathammal, R. and Kalaiselvi, V., Incorporation and in vitro application of hydroxyapatite with silver and titanium dopants synthesized by wet chemical method, *J. Environ. Nanotechnol.*, 6(4), 42–46 (2017). https://dx.doi.org/10.13074/jent.2017.12.174290

Kalaiselvi, V., Mathammal, R. and Anitha, P., Synthesis and characterization of hydroxyapatite nanoparticles using wet chemical method, *Int. J. Adv. Sci. Eng.*, 4(2), 571-574 (2017). https://dx.doi.org/10.29294/IJASE.4.2.2017.571-574

Kalaiselvi, V., Mathammal, R., Vijayakumar, S. and Vaseeharan, B., Microwave assisted green synthesis of hydroxyapatite nanorods using *Moringa oleifera* flower extract and its antimicrobial applications, *Int. J. Vet. Sci. Med.*, 6(2), 286–295 (2018). https//dx.doi.org/10.1016/j.ijvsm.2018.08.003

Kalaiselvi, V., Mathammal., R. and Anitha, P., Sol-Gel mediated synthesis of pure hydroxyapatite at different temperatures and silver substituted hydroxyapatite for biomedical applications, *J. Biotechnol. Biomater.*, 7(4), 275-277 (2017). https://dx.doi.org/10.4172/2155-952X.1000275

Mohammadi, Z. and Dummer, P. M. H., Properties and applications of calcium hydroxide in endodontics and dental traumatology, *Int. Endod. J.*, 44(8), 697–730 (2011). https://dx.doi.org/10.1111/j.1365-2591.2011.01886.x

Nikalje, A. P., Nanotechnology and its applications in medicine, *Med. Chem.*, 5(2), 81- 89(2015). https://dx.doi.org/10.4172/2161-0444.1000247

Ratanatawanate, C., Bui, A., Vu, K. and Balkus, K. J., Low-temperature synthesis of copper(II) sulfide quantum dot decorated TiO_2 nanotubes and their photocatalytic properties, *J. Phys. Chem. C.*, 115(14), 6175–6180 (2011). https://dx.doi.org/10.1021/jp109716q

Shi, Z., Huang, X., Cai, Y., Tang, R. and Yang, D., Size effect of hydroxyapatite nanoparticles on proliferation and apoptosis of osteoblast-like cells, *Acta Biomater.*, 5(1), 338–345 (2009). https://dx.doi.org/10.1016/j.actbio.2008.07.023

Simon, A. T., Dutta, D., Chattopadhyay, A. and Ghosh, S. S., Copper nanocluster-doped luminescent hydroxyapatite nanoparticles for antibacterial and antibiofilm applications, *ACS Omega*, 4(3), 4697–4706 (2019). https://dx.doi.org/10.1021/acsomega.8b03076

Uota, M., Arakawa, H., Kitamura, N., Yoshimura, T., Tanaka, J. and Kijima, T., Synthesis of high surface area hydroxyapatite nanoparticles by mixed surfactant-mediated approach, *Langmuir*, 21(10), 4724–4728 (2005). https://dx.doi.org/10.1021/la050029m

Venkatasubbu, G. D., Ramasamy, S., Avadhani, G. S., Ramakrishnan, V. and Kumar, J., Surface modification and paclitaxel drug delivery of folic acid modified polyethylene glycol functionalized hydroxyapatite nanoparticles, *Powder Technol.*, 235, 437–442 (2013). https://dx.doi.org/10.1016/j.powtec.2012.11.003